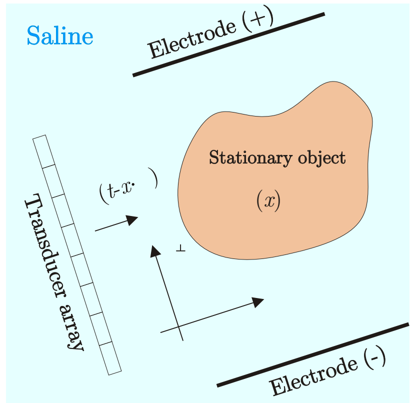

Figure 1: The novel MAET scheme; the electrode/transducer assembly rotates around the object

1 Open problems in MAET

High-resolution imaging of electrical conductivity in biological tissues is seeing as a potential breakthrough in diagnostics of breast cancer and other medical conditions associated with sharp changes in bioimpedance. Indeed, the strong contrast in the conductivity of healthy and malignant breast tissues has been reported in [1]. At the frequency 1MHz the conductivities of malignant breast samples are typically in the range of 0.8-1.4 S/m, comparing to normal tissue between 0.1-0.2 S/m [2], implying at least 4-fold contrast. Hence, the significant interest in conductivity imaging.

The first modality designed for such imaging was Electrical Impedance Tomography (EIT) [3, 4]. However, EIT can only produce low resolution images due to the well-known ill-posedness of the underlying inverse problem [5]. MAET (also known as Hall Effect Imaging or Lorentz force impedance tomography) uses the coupling of electric current to ultrasound with the intent to overcome the severe instability of EIT [6–10]. In MAET one measures the electrical potential arising when an acoustic wave propagates through conductive medium placed in a magnetic field. The Lorentz force resulting from the motion of free ions (and/or electrons) in the magnetic field causes separation of charges and, thus, generates Lorentz currents within the tissues. The electric potential associated with these currents spreads over the conductive tissues. Depending on a particular implementation, the potential is picked up by electrodes that are either placed directly on the surface of the object of interest or are submerged into conductive saline surrounding it. Then, an inverse problem needs to be solved to reconstruct the conductivity map within the tissues from the time-dependant measurements of the potential.

In detail, it has been shown ([10]) that when the tissue with conductivity $\sigma(x)$ moves with velocity $\mathbf{V}(t,x)$ within magnetic field $\mathbf{B}$, the arising Lorentz force will generate Lorentz currents $\mathbf{J}^L(t,x)$ given by the formula

$$\mathbf{J}^L(t,x) = \sigma(x)\mathbf{B} \times \mathbf{V}(t,x). \tag{1}$$

It can be further shown [11] that the difference of potentials $M(t)$ measured by a pair of electrodes can be expressed as follows

$$M(t) = \frac{1}{\rho} \int\limits_{\Omega} \varphi(t,x)\mathbf{B} \cdot \nabla \times \mathbf{I}(x)dx, \tag{2}$$

where $\mathbf{I}(x)$ is the lead current of the electrode pair (this notion is further explained below), ρ is the density of the soft tissues assumed here to be constant, and $\varphi(t,x)$ is the velocity potential. The latter potential is a solution of the wave equation (**??**); the pressure $p(t,x)$ and the velocity $\mathbf{V}(t,x)$

are expressed through $\varphi(t,x)$ as follows

$$\mathbf{V}(t,x) = \frac{1}{\rho}\nabla\varphi(t,x), \qquad p(t,x) = \frac{\partial}{\partial t}\varphi(t,x).$$

The integration domain Ω in (2) is the object of interest if the electrodes are attached directly to it. Otherwise, Ω is a larger volume that includes the conductive saline in which the object is immersed. The lead current $\mathbf{I}(x)$ mentioned above is the current that would flow through the object in the absence of the magnetic and acoustic excitation, if a unit potential difference were applied to the electrode pair. This quantity appears in (2) because $\mathbf{I}(x)$ also describes the sensitivity of the measuring system to a dipole placed at the point x.

1.1 MAET with moving electrodes

In order to obtain enough information to reconstruct the image representing the spatial distribution of conductivity $\sigma(x)$, one needs to the repeat measurements using a large family of acoustic excitations $\varphi_\omega(t,x)$ where ω is the parameter defining different excitations. For example, ω can describe the position and orientation of the ultrasound transducer. Let us denote the corresponding measurements $M_\omega(t)$.

In existing mathematical treatments of MAET one assumes that one can move the transduser(s) around the object without disturbing the current $\mathbf{I}(x)$. In this case the problem of finding the source term $\mathbf{B}\cdot\nabla\times\mathbf{I}(x)$ from measurements $M_\omega(t)$ would be equivalent to the inverse source problem of TAT/PAT mentioned above. Then the second step of the image reconstruction would consist of finding sought conductivity $\sigma(x)$ from the term $\mathbf{B}\cdot\nabla\times\mathbf{I}(x)$ [8, 11].

Unfortunately, there is no *experimentally* successful implementations of MAET that would follow the above two-step scheme. The difficulty here, which has not been addressed in literature, is the unwanted interaction of the ultrasound with the electrodes of the MAET acquisition system. Such an interaction occurs if/when the ultrasound wave hits the electrodes; it produces a strong extraneous signal (both due to the Lorentz force and to the so-called vibrational electrode potential). This signal results in a strong distortion of the useful information. This makes impossible to rotate the transducer around the object, as required by the commonly considered theoretical model.

We propose to study an alternative experimental setup where one keeps electrodes fixed related to the transducer (and away from the ultrasound beam), and rotates the electrode/transducer assembly around the object, as shown in Figure 1. In this case the current $\mathbf{I}$ is a function of both x and ω, $\mathbf{I} = \mathbf{I}_\omega(x)$, since the position of electrodes changes relative to the object. Correspondingly the source term in (2), namely $\mathbf{B}\cdot\nabla\times\mathbf{I}_\omega(x)$, is also a function of ω. In this case the previously proposed two-step MAET image reconstruction procedures are no longer applicable, and a significantly more complex inverse problem needs to be solved. As described below in Section 2, under certain assumptions this problem reduces to the problem of inverting the weighted Radon transforms of vector fields. This area of vector field tomography is quite open. We thus propose in Section 2 to develop the theory of such transforms, to find explicit inversion formula for the case of linear weights, and to apply these results to solve the MAET problem with moving electrodes.

2 Proposed work on MAET and vector field tomography

2.1 Why MAET requires the vector field approach

We consider the novel acquisition scheme for MAET, with a rotating electrode/transducer assembly, as shown in Figure 1. The object under investigation is immersed in conductive saline, and the assembly rotates around it. For simplicity, we model the propagation of currents in this scheme assuming that the electrodes are large and are placed far away from the object. Here, the conductive medium is presumed to occupy all of $\mathbb{R}^2$, with the conductivity $\sigma(x)$ being constant and known outside of the support Ω of the inhomogeneity, i.e. $\sigma(x) = \sigma_0$ for $x \in \mathbb{R}^2 \backslash \Omega$. Then the lead current $\mathbf{I}$ is a function of x and the orientation ω of the measuring assembly, i.e. $\mathbf{I} \equiv \mathbf{I}_\omega(x)$.We assume that in the absence of the inhomogeneity the electrodes generate field $E^0_\omega = \omega^\perp$ (where $\omega^\perp$ is the left normal to ω) and the corresponding potential is equal to $\omega^\perp \cdot x$. Thus, far away from the object the current is determined by the field E^0_ω in a homogeneous medium, i.e.

$$\mathbf{I}_\omega(x) = \sigma_0 E^0_\omega + o(1) = \sigma_0 \omega^\perp + o(1) \text{ as } x \to \infty.$$

Therefore in the presence of the inhomogeneity the total current is governed by the potential $u^{tot}_\omega(x) = \omega^\perp \cdot x + u_\omega(x)$ with $u_\omega(x)$ vanishing at infinity:

$$\mathbf{I}_\omega(x) = \sigma(x)\nabla u^{tot}_\omega(x) = \sigma(x)\nabla(\omega^\perp \cdot x + u_\omega(x)) = \sigma(x)\nabla u_\omega(x) + \omega^\perp \cdot \sigma(x).$$

Due to the absence of sinks and sources of charges in the medium, current $\mathbf{I}_\omega(x)$ is solenoidal, $\operatorname{div} \mathbf{I}_\omega(x) = 0$. Thus, $u_\omega(x)$ solves the divergence equation, subject to the decay at infinity

$$\nabla \cdot \sigma(x) u_\omega(x) = -\omega^\perp \cdot \nabla\sigma(x), \quad x \in \mathbb{R}^2, \tag{3}$$

$$\lim_{x\to\infty} u_\omega(x) = 0. \tag{4}$$

Let us now consider the two solutions corresponding to directions $\omega = e_1$ and $\omega = e_2$, where e_1 and e_2 are the canonical vectors in $\mathbb{R}^2$:

$$u^{(1)}(x) \equiv u^{tot}_{e_1}(x), \quad u^{(2)}(x) \equiv u^{tot}_{e_1}(x).$$

The corresponding currents will be denoted by $\mathbf{I}^{(1)}_\omega(x)$ and $\mathbf{I}^{(2)}_\omega(x)$, respectively. Due to the linearity of the problem (3), (4), the potential $u^{tot}_\omega(x)$ and current $\mathbf{I}_\omega(x)$ are linear combinations:

$$\begin{aligned} u_\omega(x) &= \omega_1 u^{(1)}(x) + \omega_2 u^{(2)}(x), \\ \mathbf{I}_\omega(x) &= \omega_1 \mathbf{I}^{(1)}(x) + \omega_2 \mathbf{I}^{(2)}(x), \quad \text{with } \omega = (\omega_1, \omega_2). \end{aligned}$$

Since MAET measurements are directly related to $\nabla \times \mathbf{I}_\omega$ (see equation (2)), let us denote by $C_\omega(x)$ the scalar curl of the two-dimensional field $\mathbf{I}_\omega(x) = (I_{\omega,1}(x), I_{\omega,2}(x))$:

$$C_\omega(x) \equiv \frac{\partial}{\partial x_1} I_{\omega,2}(x) - \frac{\partial}{\partial x_2} I_{\omega,1}(x).$$

Correspondingly, $C^{(1)}(x)$ and $C^{(2)}(x)$ are the scalar curls of $\mathbf{I}^{(1)}_\omega(x)$ and $\mathbf{I}^{(2)}_\omega(x)$, respectively. Then,

$$C_\omega(x) \equiv \omega_1 C^{(1)}(x) + \omega_2 C^{(2)}(x). \tag{5}$$

By introducing a 2D vector field $\mathbf{C}(x) \equiv (C^{(1)}(x), C^{(2)}(x))$ we re-write equation (5) as:

$$C_\omega(x) = \omega \cdot \mathbf{C}(x).$$

Let us re-formulate the inverse problem of MAET arising from our novel measuring scheme as a problem of vector tomography. Since the vector of magnetic induction $\mathbf{B}$ is perpendicular to the plane, according to (2) measurement $M_\omega(t)$ in the position defined by ω is given by the formula

$$M_\omega(t) = \frac{|\mathbf{B}|}{\rho} \int\limits_\Omega \varphi_\omega(t,x) C_\omega dx = \frac{|\mathbf{B}|}{\rho} \int\limits_\Omega \varphi_\omega(t,x) \omega \cdot \mathbf{C}(x) dx,$$

where $\varphi_\omega(t,x)$ is the velocity potential generated by the transducer located and oriented as determined by ω. Let us assume in addition that $\varphi_\omega(t,x)$ is an ideal plane wave $\varphi_\omega(t,x) = \delta(t - x\cdot\omega)$. This is the simplest realistic model: it satisfies the wave equation, it assumes that the transducer has an infinite bandwidth, and it gives rise to the velocity field that integrates to zero (as it should, since after the pulse the transducer surface returns to the original position). Then

$$M_\omega(t) = \frac{|\mathbf{B}|}{\rho}\int\limits_{\Omega} \delta(t - x\cdot\omega)\omega\cdot\mathbf{C}(x)dx. \tag{6}$$

This formula has the form of a transversal Radon transform (see Section 2.2) of field $\mathbf{C}(x)$.

We have considered above a simplified 2D MAET acquisition scheme, in order to make presentation clear and because full 3D MAET scanning have not been reported yet. However, if one considers a fully 3D MAET acquisition with moving electrode-transducer assembly, the result can be similarly formulated in terms of the transversal Radon transform of a 3D vector field.

In 2D the transversal Radon transform coincides with a better studied ray transform of a vector field. However, for both transforms the standard theoretical result is negative. Namely, any integrable solenoidal field lies in the null space of the transversal Radon and ray transforms. For our MAET application this result is not satisfactory at all, since there is no reason for $\operatorname{div}\mathbf{C}(x)$ being negligible. In order to make our inverse problem solvable, we propose to supplement the measurements by using excitations in the form of linearly modulated ultrasound waves. Namely, functions in the form $\left(x\cdot\omega^\perp\right)\eta(t - x\cdot\omega)$ are easily seen to satisfy the wave equation. They can be generated in a number of ways. For example, if a transducer array is used for sound generation (as in [12]), such waves can be obtained by scaling linearly the excitation voltage along the transducer elements. If a synthetic flat detector is utilized (as in [13]), one obtains the desired result by a weighted averaging of individual measurements. Such sound waves can also be excited using optically generated ultrasound [14,15]. As a result, we would measure integrals $N_\omega(t)$ in the form

$$N_\omega(t) = \frac{|\mathbf{B}|}{\rho}\int\limits_{\Omega} (\omega^\perp\cdot\mathbf{x})\delta(t - x\cdot\omega)\omega\cdot\mathbf{C}(x)dx. \tag{7}$$

We will refer to such a transform (and it's higher-dimensional generalizations) as a transversal Radon transform with a linear weight. Such transforms have not been studied in literature. In the next section, we propose to investigate the weighted transversal Radon transforms in a general multidimensional case, and to show that such Radon transforms can be inverted by an explicit formula. This result will enable us to solve the inverse problem of MAET presented above.

2.2 Weighted Radon transforms of vector fields

There is a significant body of work on vector and tensor tomography [16–20]. However, most of the results are related to the ray transforms (that involve integration over straight lines) of vector and tensor fields. Moreover, the only weighted transforms studied are the ray transforms, with most of the results [21–24] obtained for the exponential and attenuated ray transforms. There are only two papers [25,26] where momentum ray transforms are considered. But the MAET problem we consider reduces to the weighted and unweighted Radon transforms (with integration done over hyperplanes). A few existing works on the Radon transforms of vector fields [27,28] are restricted to unweighted transforms and to the case of potential fields whose potentials are finitely supported. This class of fields is too narrow, thus motivating the work proposed below.

An important tool in the vector tomography is the Helmholtz decomposition. Following [20] that is an authoritative book in this area, one considers an infinitely differentiable vector field $F(x)$

that belongs to the Schwarz class on $\mathbb{R}^d$ (i.e. decaying faster than any rational function of $|x|$). It can be decomposed in a sum of a potential and solenoidal parts, $F(x) = F^{\mathrm{s}}(x) + F^{\mathrm{p}}(x)$, with

$$F^{\mathrm{p}}(x) = \nabla\varphi(x), \text{ and } \operatorname{div} F^{\mathrm{s}}(x) = 0, \text{ where } \Phi(x) \equiv \Delta\varphi(x) = \operatorname{div} F^{\mathrm{p}}(x).$$

These parts $F^{\mathrm{s}}(x)$, $F^{\mathrm{p}}(x)$ are defined in all of $\mathbb{R}^d$ even if the field F itself is finitely supported; their behavior at infinity is important for further analysis.

Let us require potential $\varphi(x)$ to vanish at infinity. Then $\varphi(x)$ is unique and given by the formula:

$$\varphi(x) = (\Phi * G)(x) = \int_{\Omega} \Phi(y)G(x-y)dy$$

where $G(x)$ is the fundamental solution for the Laplace equation in $\mathbb{R}^d$:

$$G(x) = \frac{1}{2\pi}\ln|x| \text{ for } d=2, \qquad G(x) = -\frac{\Gamma(d/2-1)}{4\pi^2}|x|^{2-d} \text{ for } d \geq 3.$$

The following estimate on the behavior of F^{s} is given by Theorem 2.6.2 of [20]:

$$|F^{\mathrm{s}}(x)| \leq C(1+|x|)^{1-d}, \tag{8}$$

with the similar bound on F^{p}. While this result is general and also holds for tensor fields, it does not allow to introduce the Radon transforms of F^{s} and F^{p} in general, since the rate of decay (8) does not guarantee the existence of integrals over hyperplanes of dimension $d-1$. This might be the reason why previous works on the Radon transform of vector fields [27, 28] consider a very restrictive case of potential fields with finitely supported potential φ.

However, for general compactly supported vector fields F we can prove a stronger estimate

$$|F^{\mathrm{s}}(x)| \leq C_1(1+|x|)^{-d}, \qquad |F^{\mathrm{p}}(x)| \leq C_2(1+|x|)^{-d}. \tag{9}$$

Such a rate of decay allows one to define the Radon transform of both components $F^{\mathrm{s}}(x)$ and $F^{\mathrm{p}}(x)$ and to develop a general and elegant theory of the weighted Radon transforms of vector fields. (The PI will also work on extending estimate (9) to vector fields of the Schwarz class).

Let us consider a smooth vector field $F(x)$ finitely supported in a simply-connected and bounded region Ω in $\mathbb{R}^d$, $d \geq 2$. We extend $F(x)$ by zero to the whole of $\mathbb{R}^d$. (Although F is finitely supported, the results below use the integrability of F^{s} and F^{p} due to (9)). For any fixed value of the unit vector $\omega \in \mathbb{S}^{d-1}$, we arbitrarily extend ω to an orthonormal basis $\omega, \omega_1, ..., \omega_{d-1}$ of $\mathbb{R}^d$, where $\omega_j = \omega_j(\omega)$, $j = 1, ..., d-1$. To simplify the notation, below we will suppress the dependence of ω_j's on ω. For a given ω and $p \in \mathbb{R}$ we define a hyperplane $\Pi(\omega, p)$ by the equation $\omega \cdot x = p$. The Radon transform of the scalar function $f(x)$ is defined as

$$[\mathcal{R}f](\omega, p) \equiv \int_{\Pi(\omega,p)} f(x)\, dA_{\Pi}(x),$$

where $dA_{\Pi}(x)$ is the standard volume element on $\Pi(\omega, p)$. The Radon transform of a vector field $F(x)$ is understood component-wise, i.e. if $F(x) = (f_1(x), ..., f_d(x))$ then $[\mathcal{R}\mathcal{F}](\omega, p) \equiv (\mathcal{R}f_1, .., \mathcal{R}f_d)(\omega, p)$. Now the transversal Radon transform $\mathcal{D}^{\perp}$ of $F(x)$ can be defined as follows

$$\left[\mathcal{D}^{\perp}F\right](\omega, p) \equiv \int_{\Pi(\omega,p)} F(x)\cdot\omega\, dA_{\Pi}(x), \quad \omega \in \mathbb{S}^{d-1}, \quad p \in \mathbb{R}.$$

It would be nice to be able reconstruct $F(x)$ from the known values of $\mathcal{D}^{\perp}F$. However, since solenoidal fields F^{s} lie in the null space of $\mathcal{D}^{\perp}$, additional data are needed. Motivated by the problem of MAET discussed in Section 2.1), we supplement the values of $\mathcal{D}^{\perp}$ with weighted transversal transforms $\mathcal{W}_k$ defined by the formula

$$[\mathcal{W}_k F]\,(\omega,p) \equiv \int\limits_{\Pi(\omega,p)} (\omega_k \cdot x) F(x) \cdot \omega \, dA_{\Pi}(x), \quad k = 1, ..., d-1.$$

The above transforms contain additional linear weights $(\omega_k \cdot x)$ for two reasons. First, such transforms can be measured in our formulation of MAET. Second, as we will prove, the knowledge of $\mathcal{D}^{\perp}F$ and $\mathcal{W}_k F$, $k = 1, ..., d-1$, provides enough information to reconstruct $F(x)$ by an explicit and theoretically exact formula. One starts by relating the Radon transform of the divergence Φ of F to $\mathcal{D}^{\perp}F$. reconstructed from the transversal transform:

$$[\mathcal{R}\Phi]\,(\omega,p) = \frac{\partial}{\partial p}\left[\mathcal{D}^{\perp}F\right](\omega,p), \qquad \Phi(x) \equiv \operatorname{div} F(x).$$

Thus, Φ can be obtained from $\mathcal{D}^{\perp}F$ just by inverting the Radon transform. Further, we conjecture and propose to prove the following formula that will allow one to recover the Radon transform of F and thus, explicitly reconstruct F:

$$[\mathcal{R}F](\omega,p) = \omega\left[\mathcal{D}^{\perp}F\right](\omega,p) + \sum_{k=1}^{d-1} \omega_k \left(\frac{\partial}{\partial p}\left[\mathcal{W}_k F\right](\omega,p) - [\mathcal{R}\{(\omega_k \cdot x)\Phi\}](\omega,p)\right).$$

Establishing the above formula is work in progress. During the Summer of 2021, the PI supervised an undergraduate student Ben Shearer, a participant of the Summer school for the NSF-sponsored REU program Data Driven Discovery. Under the PI's supervision Ben was able to prove a 2D version of this formula, implement the direct and inverse problems, and validate the formula in numerical simulations. The PI proposes to develop a proper theoretical foundation for the full multi-dimensional version of this formula, and to develop the image reconstruction algorithm for MAET based on measurements with linearly weighted acoustical fields. Further, the PI will investigate the performance of this technique in numerical simulations, and will try to implement it in hardware.

References

[1] Andrzej J Surowiec, Stanislaw S Stuchly, J Robin Barr, and AASA Swarup. Dielectric properties of breast carcinoma and the surrounding tissues. *IEEE Transactions on Biomedical Engineering*, 35(4):257–263, 1988.

[2] Jaewook Shin, Min Jung Kim, Joonsung Lee, Yoonho Nam, Min-oh Kim, Narae Choi, Sooyeon Kim, and Dong-Hyun Kim. Initial study on in vivo conductivity mapping of breast cancer using mri. *Journal of Magnetic Resonance Imaging*, 42(2):371–378, 2015.

[3] David C Barber and Brian H Brown. Applied potential tomography. *Journal of Physics E: Scientific Instruments*, 17(9):723, 1984.

[4] Liliana Borcea. Electrical impedance tomography. *Inverse problems*, 18(6):R99, 2002.

[5] M. Cheney, D. Isaacson, and J. C. Newell. Electrical impedance tomography. *SIAM Rev.*, 41:85–101, 1999.

[6] Han Wen, Jatin Shah, and Robert S Balaban. Hall effect imaging. *IEEE transactions on biomedical engineering*, 45(1):119–124, 1998.

[7] Pol Grasland-Mongrain, J-M Mari, J-Y Chapelon, and Cyril Lafon. Lorentz force electrical impedance tomography. *Irbm*, 34(4-5):357–360, 2013.

[8] Bradley J Roth and Kevin Schalte. Ultrasonically-induced lorentz force tomography. *Medical & biological engineering & computing*, 47(6):573–577, 2009.

[9] Reyhan Zengin and Nevzat Güneri Gençer. Lorentz force electrical impedance tomography using magnetic field measurements. *Physics in Medicine & Biology*, 61(16):5887, 2016.

[10] Amalric Montalibet, J Jossinet, A Matias, and D Cathignol. Electric current generated by ultrasonically induced lorentz force in biological media. *Medical and Biological Engineering and Computing*, 39(1):15–20, 2001.

[11] Leonid Kunyansky. A mathematical model and inversion procedure for magneto-acousto-electric tomography. *Inverse problems*, 28(3):035002, 2012.

[12] Tong Sun, Penghui Hao, Chien Ting Chin, Dingqian Deng, Tiemei Chen, Yi Chen, Mian Chen, Haoming Lin, Minhua Lu, Yi Gao, et al. Rapid rotational magneto-acousto-electrical tomography with filtered back-projection algorithm based on plane waves. *Physics in Medicine & Biology*, 66(9):095002, 2021.

[13] L Kunyansky, CP Ingram, and RS Witte. Rotational magneto-acousto-electric tomography (MAET): Theory and experimental validation. *Physics in Medicine & Biology*, 62(8):3025, 2017.

[14] Hui Xia, Guangxin Ding, and Guoqiang Liu. Magneto-acousto-electrical tomography with magnetic induction based on laser-generated ultrasound transducer. *Journal of Medical Imaging and Health Informatics*, 9(1):183–187, 2019.

[15] Guangxin Ding, Hui Xia, Xiaonan Li, and Guoqiang Liu. Experimental study of magneto-acousto-electrical tomography based on laser-generated ultrasound technology. In *Tenth International Conference on Information Optics and Photonics*, volume 10964, page 109646A. International Society for Optics and Photonics, 2018.

[16] Stephen J Norton. Tomographic reconstruction of 2-d vector fields: application to flow imaging. *Geophysical Journal International*, 97(1):161–168, 1989.

[17] Stephen J Norton. Unique tomographic reconstruction of vector fields using boundary data. *IEEE Transactions on image processing*, 1(3):406–412, 1992.

[18] Gunnar Sparr and Kent Stråhlén. Vector field tomography: an overview. *IMA Volumes in Mathematics and its Applications; Computational Radiology and Imaging: Therapy and Diagnostic*, 110, 1998.

[19] Thomas Schuster. 20 years of imaging in vector field tomography: a review. In *Mathematical Methods in Biomedical Imaging and Intensity-Modulated Radiation Therapy (IMRT)*, volume 7. (CRM), Birkhäuser, 2008.

[20] Vladimir Altafovich Sharafutdinov. *Integral geometry of tensor fields*, volume 1. Walter de Gruyter, 2012.

[21] Kent Stråhlén. Exponential vector field tomography. In *International Conference on Image Analysis and Processing*, pages 348–355. Springer, 1997.

[22] Alexander A Bukhgeim and Sergey G Kazantsev. Full reconstruction of a vector field from its attenuated vectorial radon transform. In *Modelling, Identification and Control*, pages 294–298, 2003.

[23] F Natterer. Inverting the attenuated vectorial radon transform. *J. Inverse Ill-posed Problems*, 13(1):893–101, 2005.

[24] Guillaume Bal. On the attenuated radon transform with full and partial measurements. *Inverse Problems*, 20(2):399, 2004.

[25] Venkateswaran P. Krishnan, Ramesh Manna, Suman Kumar Sahoo, and Vladimir A. Sharafutdinov. Momentum ray transforms. *Inverse Problems and Imaging*, 13(3):679–701, 2019.

[26] Rohit Kumar Mishra. Full reconstruction of a vector field from restricted doppler and first integral moment transforms in rn. *Journal of Inverse and Ill-posed Problems*, 28(2):173–184, 2020.

[27] A Polyakova. Reconstruction of a vector field in a ball from its normal radon transform. *Journal of Mathematical Sciences*, 205(3), 2015.

[28] AP Polyakova and IE Svetov. Numerical solution of the problem of reconstructing a potential vector field in the unit ball from its normal radon transform. *Journal of Applied and Industrial Mathematics*, 9(4):547–558, 2015.